Research Article

# Morphology and mineralogy of ambient particulate matter over mid-Brahmaputra Valley: application of SEM–EDX, XRD, and FTIR techniques

**Jayanta Bora**[1] · **Pratibha Deka**[1] · **Pranamika Bhuyan**[1,2] · **Kali Prasad Sarma**[1] · **Raza Rafiqul Hoque**[1]

## Abstract

Ambient particulate matter (PM), collected during a dust event over mid-Brahmaputra Valley of India, was characterized. The PM samples were analyzed using scanning electron microscopy–energy-dispersive X-ray spectroscopy (SEM–EDX), X-ray diffraction (XRD), and Fourier transform infrared spectroscopy (FTIR) techniques. The SEM micrographs revealed varied shapes of the PM, viz. spherical, irregular, angular, cluster, flaky, rod-like, crystalline and agglomerate structures indicating the probable nature of their sources and formation as biogenic, geogenic, or anthropogenic. Some biogenic particles like plant materials, pollens, and diatoms were captured under SEM. The presence of diatom in PM samples was indicative of wind-blown dust from the dried bed of the Brahmaputra River. The honeycomb-like structures of brochosomes secreted by the leafhoppers of the Cicadellidae family were also captured. On the contrary, the background sample had mostly carbonaceous particles. The XRD and FTIR analyses indicated the presence of quartz, feldspar, kaolinite, illite, augite, and calcium aluminum silicate, cerussite, calcite, montmorllonite, and organic carbon. The airmass backward trajectory analysis explained the local contribution of the dust.

**Keywords** Particulate matter · Morphology · Mineralogy · SEM–EDX · XRD · FTIR

## 1 Introduction

Atmospheric particulate matter (PM) plays a vital role in the global climate system [1]. It directly affects the climate through the processes of scattering, transmission, and absorption of solar radiation. PM acts as cloud condensation nuclei (CCN), thereby indirectly affecting the climate system [2]. The chemical nature of the PM impacts the CCN processes. PM also adversely impacts human health [3]. Due to its effects on human health and the environment, PM has been listed as a criteria air pollutant by countries worldwide to regulate it for its control [4]. Inhalation of organic species and heavy metals associated with the fine particles ($PM_{2.5}$: PM ≤ 2.5 μm) causes serious health effects [5]. Bioaerosols also adversely affect humans, animals, and plants [6].

Morphology and composition have a bearing on their physical, chemical, and optical properties [7]. These properties undergo change with respect to space and time and differentially affect human health, visibility, and energy balance on a regional scale [8 and references therein]. Detailed characterization of individual atmospheric particles is indicative of their sources of origin, transportation, and removal [9]. Morphology and chemical composition

✉ Pratibha Deka, pratibhadeka@gmail.com | [1]Department of Environmental Science, Tezpur University, Tezpur 784028, India. [2]Department of Environmental Studies, Assam Women's University, Jorhat 785004, India.

of the particles control their settling velocity by applying a drag force and hence affect the transportation process of the particles [10, 11]. Morphological characteristics like shape, surface roughness, and edge sharpness affect the scattering property of a particle [12]. The chemistry of PM is also the driver of the climatic effects of PM [13].

The carbonaceous aerosols play a greater role in absorbing and scattering the incoming solar radiations and also indirectly affecting the hydrological cycle [14]. The morphology of carbonaceous aerosols is also a key attribute considered while calculating the global warming contribution of carbonaceous particles [15].

The mineral dust particles are an important constituent of atmospheric aerosols and are contributors to total atmospheric aerosol loading. Mineral dust makeup to about 40% of global aerosol emissions from natural sources [16]. They help in the removal, deposition, and transport of atmospheric pollutants [17] including the reduction in the levels of ambient ozone to an extent of 5.5% [18]. Mineral aerosol particles carried by dust storms can be transported to a long distance, which may have impacts of regional and global scales [19].

Characterization of dust aerosols reveals important information on their source of origin [20, 21]. Mineralogical, chemical, and physical results of mineral dust could provide useful information for applications in climate modeling, visibility, remote sensing, medical geology, and other studies [22], as the heterogeneous composition of mineral aerosols increases the uncertainty in atmospheric climate models [23].

Dust events add lots of crustal aerosol to the atmosphere, which alters radiation balance when present in higher concentrations [24]. It leads to a decrease in the number of accumulation particles, an increased number of coarse particles, and a favorable condition for new particle formation [25]. Among the sources of dust particles in the atmosphere, rivers are one of the important sources of atmospheric dust particles [26]. The Brahmaputra River of Assam is a trans-boundary river flowing through Tibet, India, and Bangladesh. Earlier studies reported the Aerosol Optical Depth (AOD) over Brahmaputra Valley attributed to dust aerosols [27, 28] and also reported crustal dust and soil resuspension as important sources of $PM_{10}$ (PM ≤ 10 µm) over the mid-Brahmaputra Valley [29, 30]. Detailed studies on the characterization of particulates during dust events of this region was lacking. Therefore, the present study was taken up and so designed to investigate the physicochemical attributes of atmospheric particulates during a dust event.

## 2 Experimental methods

### 2.1 Study site

The study was carried out at Tezpur University, a rural residential institutional area (26°37′ N and 92°50′ E) (Fig. 1). Tezpur is situated on the north bank of the Brahmaputra River and represents the regions around the middle stretch of the river in India. The region is mostly rural with agricultural lands, forests, tea plantations, riverine, and marshy areas. Many small-scale industries that run on coal and wood like tea processing units, brick kilns, auto work stations, and minor agriculture-based industries are growing in the region with time. Moreover, two major national highways NH 15 and NH 715 meet at a point and pass through Tezpur.

### 2.2 Collection of PM

The collection of PM was done by a fabricated grab sampler with an airflow rate of 1.2 L/min. Sampling was carried out at the rooftop of the Department of Environmental Science building, Tezpur University, at a height of 20 m from the ground. The collections were made on 47 mm diameter Whatman Glass Fiber filters, Grade GF/A for morphology study and on polytetrafluoroethylene (PTFE) membrane filters for XRD and FTIR analyses [31]. The pore size of Whatman glass fiber filters and PTFE membrane filter is 1.6 µm and 1.0 µm, respectively. Sampling was carried out during the four-day-long dust event of April 2013. Two sets of samples were collected—(i) 24-h samples and (ii) 3-h samples. The shorter duration samples were used for the single-particle analysis. The wind speed during the sampling period ranged from 2 ms$^{-1}$ to 9.10 ms$^{-1}$. Heavy accumulation of coarse and fine particles was found on the filter paper. A 24-h sample was also collected during the non-dusty period (3 days after a rain event during June 2013) to understand the background characteristics of PM. The details of the sampling are provided in Supplement 1.

Meteorological condition is the main driving factor controlling the distribution of air pollution in a region. In the present study, meteorological data were downloaded from wunderground.com (Supplement 2). Temperature, humidity, wind speed, and rainfall data during the sampling days are provided in Supplement 2. No rainfall was recorded in April 2013.

### 2.3 Analyses

A square of the sample filters (1 mm × 1 mm) was cut and coated with platinum for the morphological analysis under

**Fig. 1** **a** The study area (Tezpur) in the Brahmaputra Valley and the neighboring regions of Asia, **b** Tezpur locality and sampling location, Tezpur University

the scanning electron microscope (SEM) (JEOL JSM 6390 LV). Energy-dispersive X-ray spectrometer (EDS) INCAx Sight microanalysis system (Oxford Instruments, Model 7582), hyphenated with the SEM, was used for elemental analysis. The silicon (lithium-drifted) crystal detector of the EDS had an acquisition rate of 50,000 cps. The Super Atmosphere Supporting Thin Window (SATW) of the detector confirms good resolution at the low energy end of the spectrum with a resolution of 137 eV at 5.9 keV. The detector had a minimum quantification limit of 0.01 wt. %. The PM deposited on the PTFE filter was used for single-particle analysis under SEM.

For the XRD analysis, samples collected on a PTFE filter were used because it is very stable and absorbs negligible water or gases [31]. The particles on the PTFE filter were scooped out using a teaser and placed in the quartz sample holder for X-ray diffractometer (XRD, Rigaku, Miniflex) analysis. The X-ray diffraction data were collected at Bragg angle $2\theta$ ranging from 10 to $80^0$ with a scanning speed of $0.05^0$ $min^{-1}$. The X-ray source was a Cu K$\alpha$ line with a wavelength of 1.54 Å. The Braggs' equation $n\lambda = 2d_{hkl}Sin\theta$ was used to calculate the interplanar spacing ($d_{hkl}$). In this equation, n is the order of reflection ($n = 1$) and $\lambda$ is the wavelength of X-ray used ($\lambda = 1.54$ Å). The peak positions ($2\theta$) and interplanar spacing ($d_{hkl}$) were compared with the Joint Committee on Powder Diffraction Standards (JCPDS), version 2.4 database for mineral identification [32].

Samples collected on PTFE filters were also used for Fourier transform infrared (FTIR) study. FTIR spectra from 400 to 4000 $cm^{-1}$ were recorded on the FTIR spectrometer (Perkin Elmer; Frontier MIR-FIR). 1 mg of dust sample was dispersed with KBr (spectroscopic grade) in the ratio of 1:20. The sample was then pelletized at a pressure of about 1 MPa before measuring the FTIR spectra. The FTIR analysis was carried out at a spectral resolution of 4 $cm^{-1}$. The reported spectrum is the average of four scans.

To trace the pathway of airmasses during the dust event, 72-h airmass back trajectories at 100 m AGL were computed using the Hybrid Single-Particle Lagrangian Integrated Trajectory (HYSPLIT) model. The reanalysis data were downloaded from the Gridded Meteorological Data Archives (ready.noaa.gov/archives.php). Geographic Information System (GIS)-based software TrajStat (http://www.meteothink.org/products/trajstat.html) was used to project the HYSPLIT back trajectory clusters using the 72-h trajectories reaching the site hourly on 1st and 3rd April 2013.

## 2.4 Quality control

Care was taken to prepare contamination-free samples. Filters were desiccated before and after the collection of samples to avoid traces of moisture. Acetone and methanol were used to clean the tweezers, scissors, and sampling stubs before each use. The sample holder of the XRD was cleaned properly before each use.

# 3 Results and discussion

## 3.1 Morphological characteristics

SEM micrographs of PM are shown in Fig. 2. Particles of various shapes and sizes—spherical, irregular, cluster, flaky, rod-like, angular, agglomerates chain, and triangular particles—are seen (Fig. 2a and b). Previous workers reported extremely irregular shapes of particles [23, 33]. Aggregation could be an important formation process of irregular shape particles [34]. SEM micrographs of aerosols collected during the non-dusty period showed greater accumulation of carbonaceous agglomerates, explicit chain-like structures, and spherical soot particles (Fig. 2c) [24, 33]. Soot particles are generally emitted from incomplete combustion of biomass and fossil fuels [7]. Carbonaceous agglomerate and chain-like structures may explain the emissions from fossil fuel combustion in vehicles and industries [24, 33]. Spherical shape particles are generally indicative of combustion processes or high-temperature processes [24], which were vividly seen in the micrographs. Thus, based on morphological expression, we have categorized the particles vis-a-vis their origins, viz. biogenic, geogenic, and anthropogenic. This is clearer from high-resolution SEM images (above 10,000×).

Clay-like structure (sheets) and fine carbonaceous spherical particles were seen (Fig. 2d). The presence of clay-like structures may explain the geogenic origin, which later resuspended from the crustal surface by the wind gust. Figure 2e shows the crustal dust with sharp-edged particles, emitted from anthropogenic construction activity and movement of vehicles on road. We also found diatoms in the bulk sample analysis (Fig. 2f). Figure 3 shows the particles of biogenic origin which include plant debris, pollen, and brochosomes secreted by leafhoppers of the family Cicadellidae—an abundant species of bioaerosols in ambient air [35]. Brochosomes are spherical, honeycomb-like nanoparticles made of proteins and lipids [36]. It acts as a water-repellent protective surface coating [35, 36]. Pollen can be transported up to 100–1000 km [37] and can also act as CCN [38]. Figure 4 shows fine particles of different origins with size measurements. Fine particles smaller than 1.5 μm were emitted from fly ash generated from combustion [24] and fine dust from construction and vehicular movement. Biogenic particles of minimum size ~ 275 nm (Fig. 3d) were also present in the samples. Spherical soot particles and irregular shape particles are seen in Fig. 4a. The spherical soot particulates could be

**Fig. 2** SEM micrographs at different magnification showing different morphologies: **a**, **b** bulk sample collected at Tezpur during dusty periods, **c** carbonaceous agglomerate and soot aerosol during non-dusty periods, after a rainfall **d** clay-like crustal matter along with spherical fly ash particles, **e** crustal dust with sharp-edged and sheet-like structures, and **f** image showing the presence of biogenic aerosols like diatom
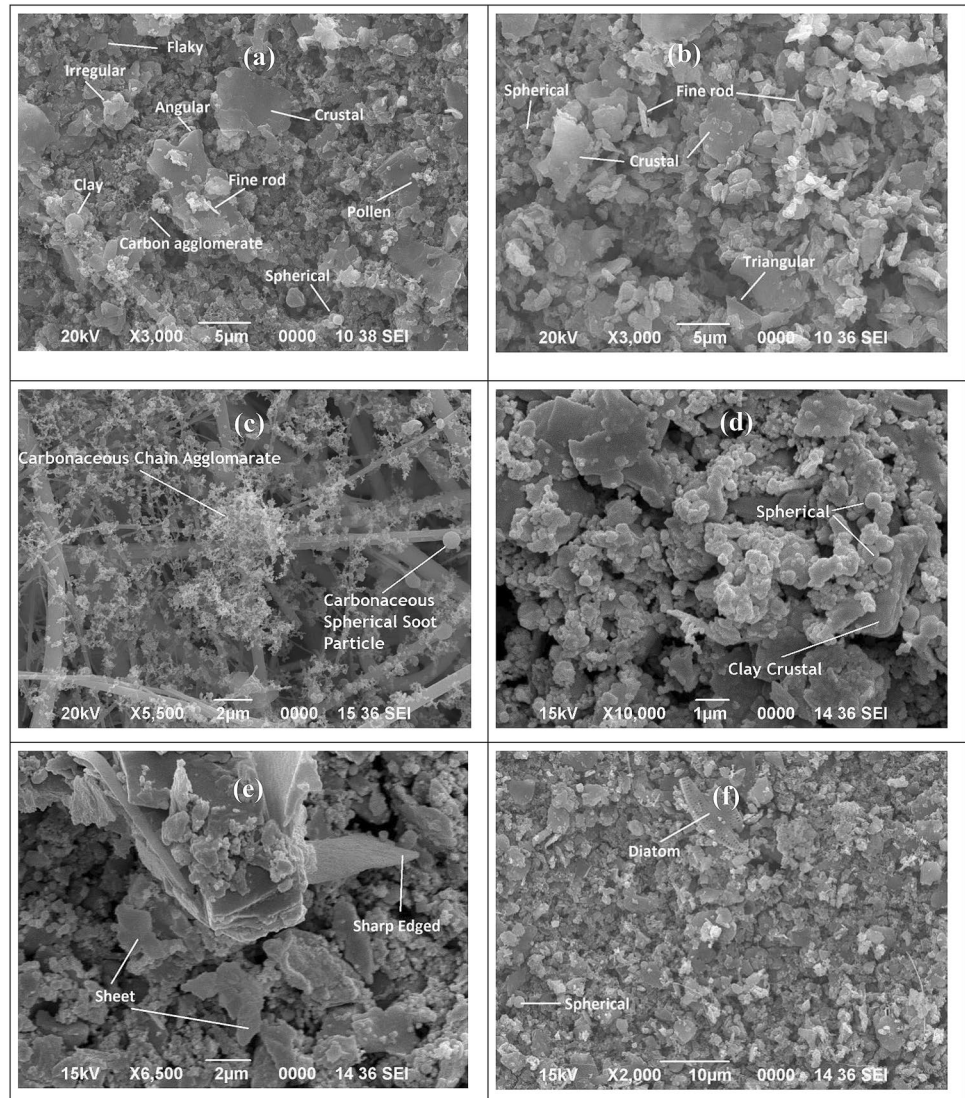


of combustion origin like coal and biomass burning [39]. There are several coal-fed brick kiln industries nearby areas of the sampling station. The irregular-shaped particles could be from crustal and construction activities. Also, soot agglomerates from vehicular emission are seen in Fig. 4b.

## 3.2 Composition using energy-dispersive X-ray (EDX) spectroscopy

Elemental analysis of bulk sample (Fig. 5a, spectrum 1) showed the following sequence of abundance: O > C > S i > Al > Fe > Ca > Na > Ti > Mg > K > S (Table 1). The carbon (C) in the PM is a product of combustion coming from biomass and/or fossil fuel burning [40, 41]. The detection of sulfur (S) and potassium (K) together with the C indicated the presence of carbonaceous soot particles which could have originated from agricultural burning or wood burning in household activities and coal burning

in factories and brick kiln industries of nearby areas [30]. The presence of oxygen (O), silicon (Si), iron (Fe), magnesium (Mg), sodium (Na), and calcium (Ca) showed a high accumulation of crustal clay minerals coming from resuspended dust (Fig. 5a). The EDX analysis of bulk samples may interfere with the compositional characteristic of particles originating from different sources. So EDX spectrum of single-particle with different morphology in the bulk sample was tried. Figure 5b shows the EDX pattern of two particles; one large particle (Fig. 5b, spectrum 1) of irregular shape with uniform surface and another small spherical shape particle (Fig. 5b, spectrum 2). Both particles contained similar elements (Al, Ca, C, Fe, Mg, Mn, Ni, O, K, Si, Na, Ti, V, and Zn) irrespective of their shape and size (Table 1). Detection of these element showed the presence of alumina silicate, mica, quartz-like minerals and carbonaceous material. Comparison of the present study with other reported works from India showed accumulation of
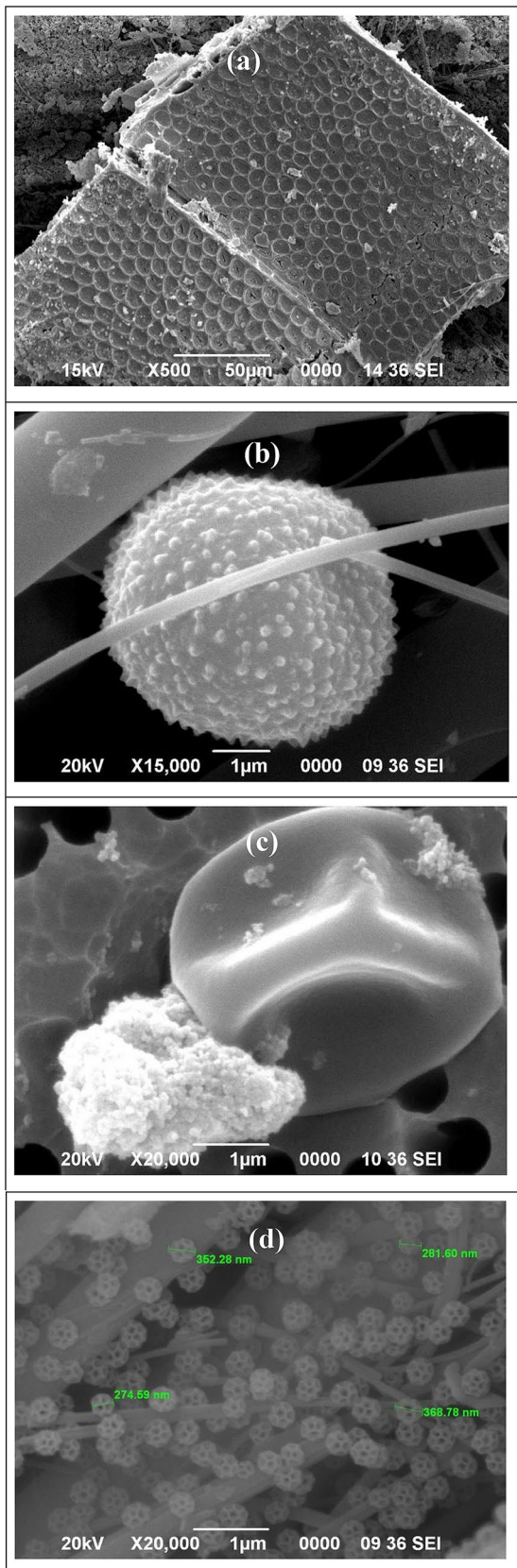
**Fig. 3** Biogenic aerosols: **a** plant parts, **b**, **c** pollen and **d** brochosomes secreted from insects
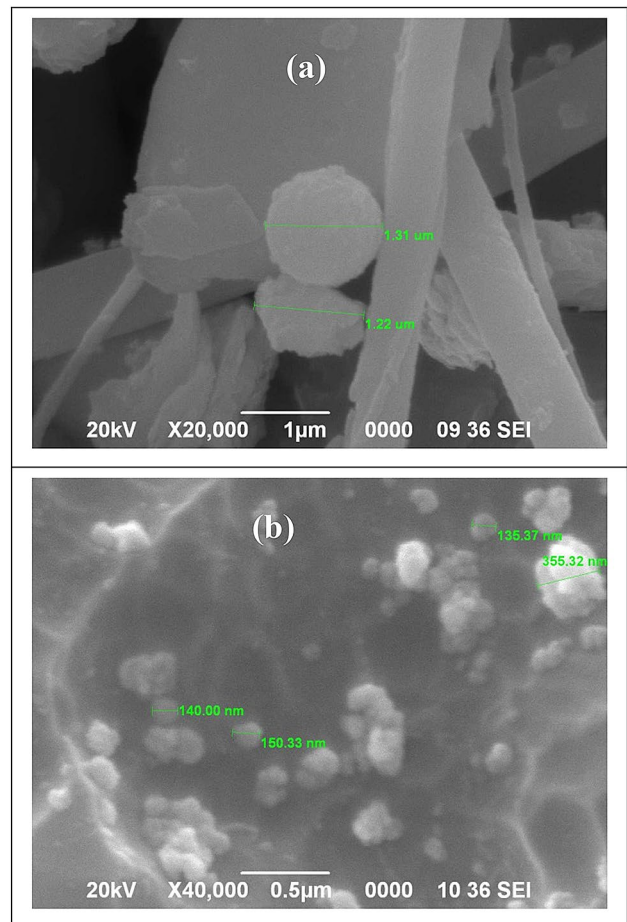
**Fig. 4** Fine particles originated from anthropogenic activities: **a** industrial and construction activities **b** soot agglomerates from vehicular emission

geogenic mineral/clay particles generated by resuspension of dust from soil/road and other anthropogenic particles from the burning of fossil fuel and biomass [31, 39, 42, 43].

The EDX analyses of single particles collected for a short duration are shown in Fig. 6, and the elemental concentrations are presented in Table 2. Mineral coarse particles with irregular shapes and carbonaceous particles were observed. Along with mineral dust particles, soot of sulfates was observed (Sample-1 spectrum-4 and Sample-2 spectrum-1). The presence of sulfur confirms their origin from the combustion process. These particles probably originated from soil dust, dust resuspension from road and earth crust, and other anthropogenic activities like construction and vehicular movement on-road, combustion activities, and agricultural fields. The irregular shaped particles are formed by two processes; (i) they may form by chemical reactions among pre-existing solid, liquid or gaseous phases, or (ii) by aggregation of pre-existing particles [34]. The elemental composition of these particles mainly
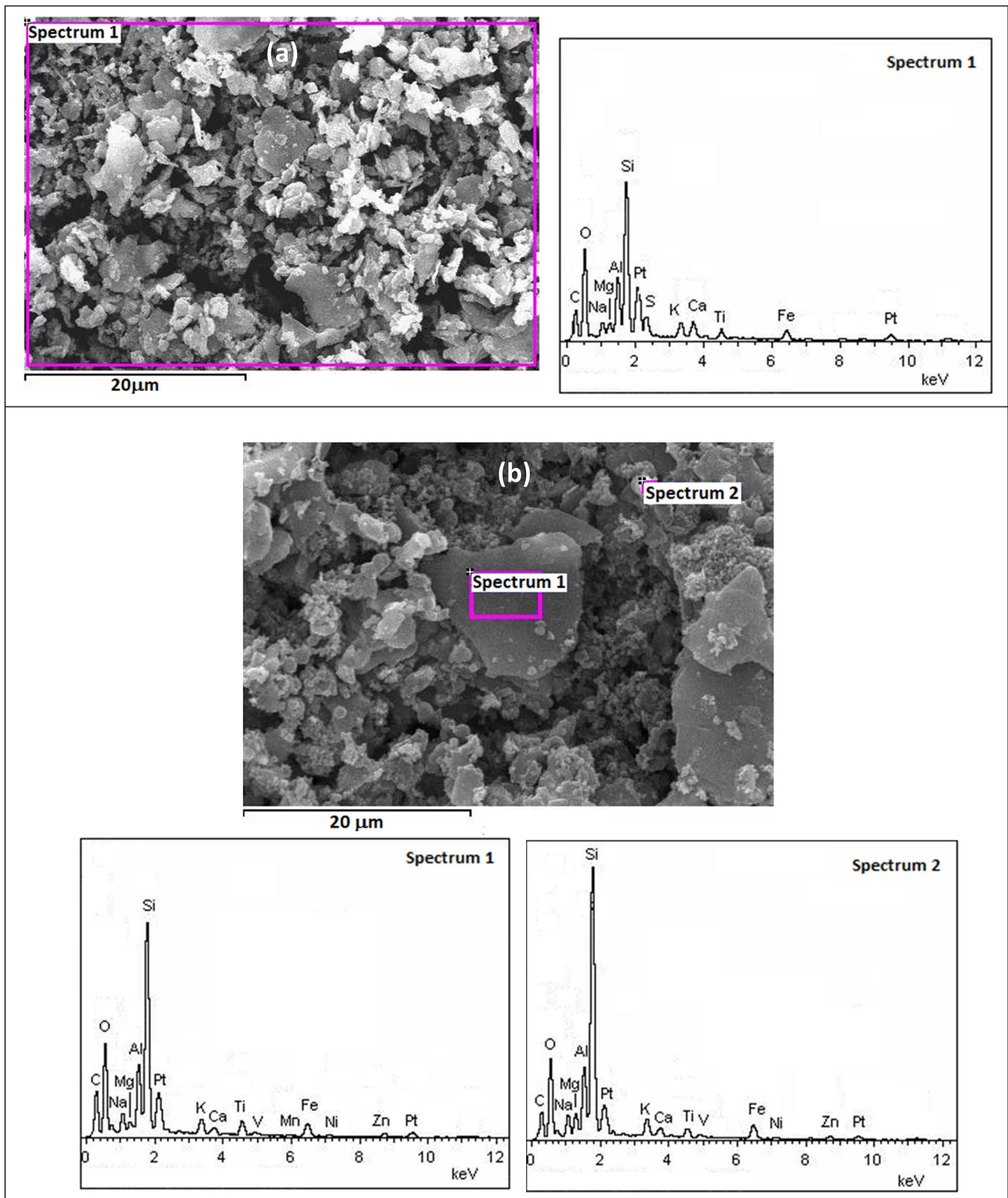
**Fig. 5** **a** SEM–EDX analysis of bulk sample **b** SEM–EDX of a large (spectrum 1) and a small (spectrum 2) particle at the bulk sample (the Pt peak was due to the coating used)

**Table 1** Elemental composition (%) of PM

| EDX taken on | Bulk sample | Coarse particle | Fine particle |
|---|---|---|---|
| Corresponding image and EDX spectrum | Figure 5a,spectrum-1 | Figure 5b,spectrum-1 | Figure 5b,spectrum-2 |
| Aluminum (Al) | 2.78 | 4.08 | 3.44 |
| Calcium (Ca) | 1.75 | 0.74 | 0.76 |
| Carbon (C) | 26.4 | 15.66 | 25.65 |
| Iron (Fe) | 1.76 | 2.29 | 2.14 |
| Magnesium (Mg) | 1.41 | 0.72 | 1.5 |
| Manganese (Mn) | | 0.26 | |
| Nickel (Ni) | | 0.09 | 0.05 |
| Oxygen (O) | 38.43 | 43.78 | 37.56 |
| Potassium (K) | 1.31 | 1.36 | 1.35 |
| Silicon (Si) | 10.71 | 14.21 | 15.21 |
| Sodium (Na) | 1.61 | 2.68 | 2.39 |
| Sulfur (S) | 0.89 | | |
| Titanium (Ti) | 1.5 | 2.05 | 1.29 |
| Vanadium (V) | | 0.08 | 0.14 |
| Zinc (Zn) | | 1.27 | 1.42 |
| Platinum (Pt)* | 11.44 | 10.74 | 7.10 |

*Pt is the coating element

consisted of Al, Si, O, C, Na, K, Fe Mg, and Ca indicating the presence of $CaCO_3$ and aluminosilicates which were most likely from geological sources (Table 2) [31, 42]. A high content of Si and Al with varying Mg, K, Fe, and Ca is characteristic of aluminosilicates [44]. The compositions of the particles with smooth spherical shape (Fig. 7a) and biogenic particle (Fig. 7b) were also analyzed, and their elemental concentrations are presented in Table 2. Figure 7a shows the presence of soot/fly ash particles emitted from various kinds of burning processes and coal combustion. Tezpur site is located in a rural area with low or no vehicular traffic, and during the pre-monsoon season (March to May) lots of coal-fed brick kilns industries remain active nearby. The fly ash particles are mainly composed of aluminosilicates and iron and/or calcium-rich particles [45]. The size of fly ash particles ranges between 2 μm and 10 μm and generally spherical [45].

Figure 7b shows a biogenic particle—a diatom. Biogenic particles such as pollen with (C+O) > 80% and a minor amount of Na, Si, Al < 10% were observed (Fig. 3). These particles also have various shapes and sizes. Single-particle analysis using SEM–EDX indicated the probable biogenic (plant parts, pollens, diatoms), geogenic (road dust, resuspended soil dust), and anthropogenic (carbonaceous particle, fly ash) origin of particles.

### 3.3 Mineralogy

Figure 8 shows the XRD pattern of PM. The broad hump of the spectra appears due to the amorphous nature of the sample and the irregular arrangement of the materials. The distinct small XRD peaks position (2θ values) along with calculated interplanar spacing ($d_{hkl}$) is provided in Table 3. The mineral peaks of quartz [46], feldspar [47], kaolinite [48], illite [49], augite [50], and calcium aluminum silicate [31] are distinctly observed.

To further confirm the presence of different minerals in the samples, FTIR analysis was carried out (Fig. 9a and b). For proper visualization of the absorption peaks, the spectrum collected was shown in two separate wave ranges: 400–1999 $cm^{-1}$ (Fig. 9a) and 2000–4000 $cm^{-1}$ (Fig. 9b) [20]. The FTIR spectrum indicated the presence of feldspar, quartz, augite, cerussite, calcite, organic carbon along with clay mineral kaolinite, illite, montmorillonite, and imogolite (Table 4). The Brahmaputra River has high abundances of feldspar, kaolinite, chlorite, illite, and quartz-like minerals [56, 57]. Kaolinite, formed from feldspar under acidic conditions, is the dominant species of the Brahmaputra River [56]. The presence of the same types of minerals in aerosol samples might indicate that dried beds of the Brahmaputra River are one of the major
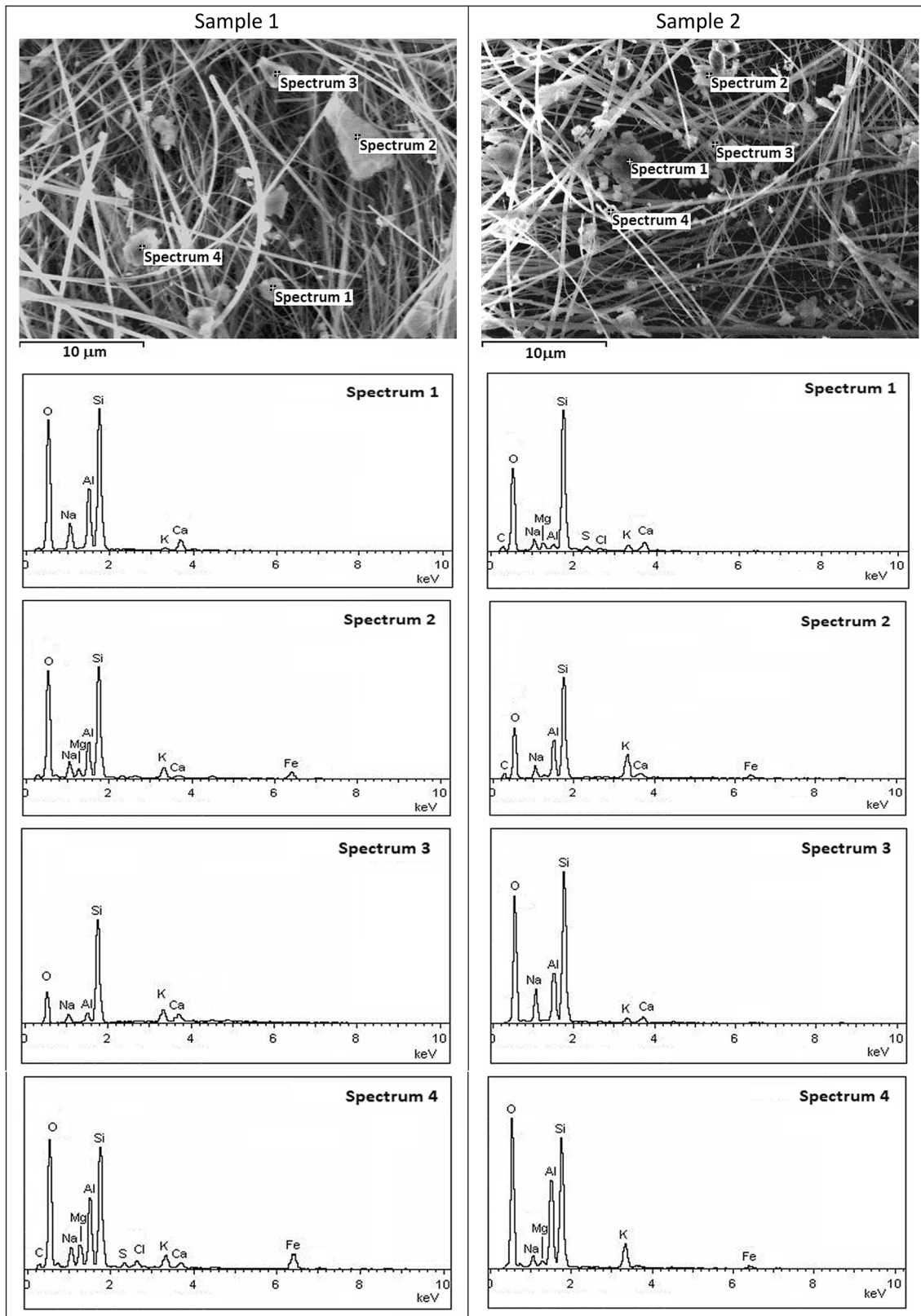
**Fig. 6** EDX analysis of single particles of two samples along with 4 different spectra of point scanning (samples collected were for a short period; 3-h sampling)

**Table 2** Elemental composition (%) of individual particles of different origin

| EDX spectrum → | Mineral particles with different size and shape | | | | | | | | Figure 7a, soot particle | Figure 7b, diatom particle |
|---|---|---|---|---|---|---|---|---|---|---|
| | Figure 6 (Sample-1) | | | | Figure 6 (Sample-2) | | | | | |
| | Spectrum-1 | Spectrum-2 | Spectrum 3 | Spectrum-4 | Spectrum-1 | Spectrum-2 | Spectrum-3 | Spectrum-4 | Spectrum-1 | Spectrum-3 |
| Aluminum (Al) | 9.05 | 6.64 | 2.91 | 8.16 | 0.70 | 7.39 | 7.65 | 11.48 | 0.46 | 0.46 |
| Calcium (Ca) | 2.50 | | 3.88 | 1.01 | 2.68 | 0.75 | 1.63 | | 0.29 | |
| Carbon (C) | | | | 8.37 | 12.88 | 12.57 | | | 64.48 | 43.87 |
| Chlorine (Cl) | | 0.63 | | 0.86 | 0.53 | | | | 0.9 | |
| Iron (Fe) | | 4.76 | | 6.77 | | 2.81 | | 1.37 | | |
| Magnesium(Mg) | | 1.73 | | 3.16 | 1.24 | | | 0.75 | | |
| Oxygen (O) | 59.38 | 57.33 | 48.08 | 50.00 | 54.82 | 45.75 | 57.24 | 60.92 | 24.87 | 46.59 |
| Potassium (K) | 0.48 | 2.79 | 6.34 | 1.93 | 1.41 | 6.53 | 1.39 | 4.39 | 0.37 | |
| Silicon (Si) | 22.41 | 21.19 | 34.30 | 15.07 | 22.14 | 20.56 | 24.18 | 18.94 | 3.98 | 9.07 |
| Sodium (Na) | 6.18 | 4.93 | 4.49 | 3.93 | 2.71 | 3.63 | 7.92 | 2.16 | 4.03 | |
| Sulfur (S) | | | | 0.74 | 1.41 | | | | 0.32 | |
| Titanium (Ti) | | | | | | | | | 0.29 | |
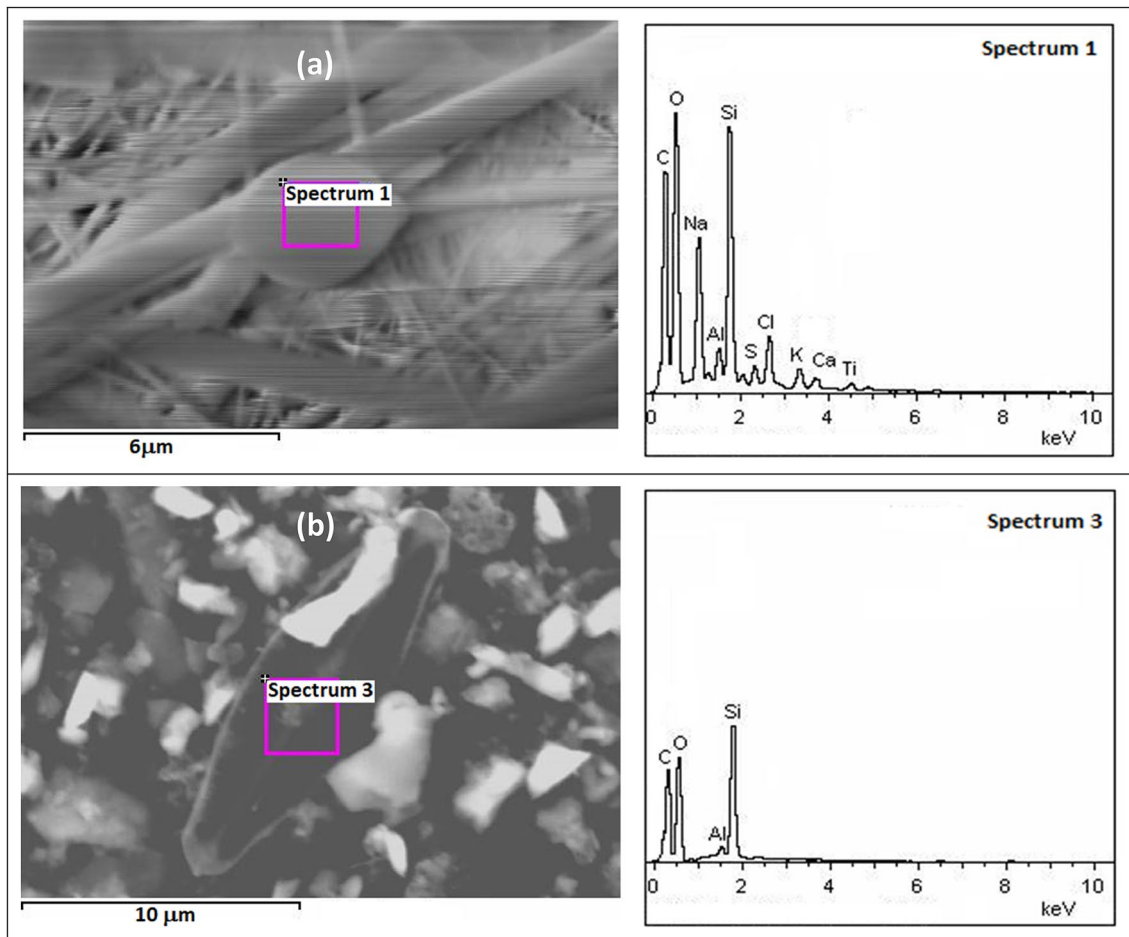


**Fig.7 a** SEM–EDX of anthropogenic soot particles with spherical morphology **b** SEM–EDX of biogenic (Diatom) particle
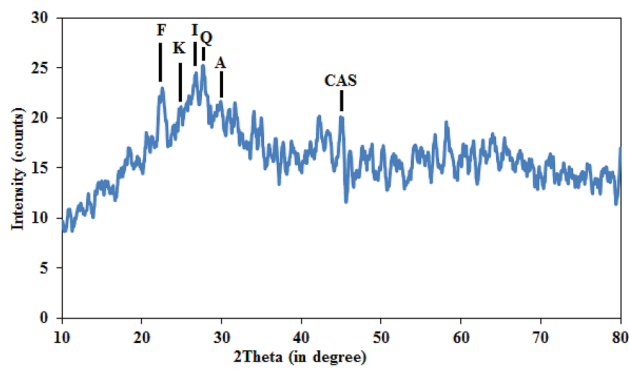
**Fig. 8** XRD pattern for the aerosol sample collected at Tezpur. Quartz (Q), feldspar (F), kaolinite (K), illite (I), augite (A) and calcium aluminum silicate (CAS)

sources of atmospheric aerosol particles during the windy events of pre-monsoon season. This is also supported by the presence of diatoms in the samples. The diatoms are a group of microalga present in freshwater and marine environments, and the Brahmaputra River is rich in diatom species [58].

Researchers had applied trajectory analysis to trace the pathway of airmasses into a region [40, 41]. The airmass backward trajectory clusters reaching the site during the dust event are shown in Fig. 10. It is explicit that local wind gusts prevailed over the region during the dust event. Saikia et al. [59] found that during the dry season the sand bar of the Brahmaputra River covered an area of 154 km$^2$ in 2014 within the length of 40 km near the Tezpur area. More so, during the dry season there is no vegetation on the open beds, which makes it easy for the aeolian removal of matter from the surface. A minimum threshold wind speed ($U$) of 6 ms$^{-1}$ is sufficient to remove a particle from the dry surfaces with < 5% vegetation cover [60]. The maximum wind speed was 9.1 ms$^{-1}$ with an average wind speed of 5 ms$^{-1}$ during the study period. This indicated the lifting of the aerosol particles from dried riverbeds of the Brahmaputra River during the windy period which could be transported to a long distance.

**Table 3** Minerals, corresponding XRD peak positions (2θ) and calculated interplanar spacing ($d_{hkl}$)

| Minerals | 2θ (degree) | $d_{hkl}$ (Å) |
|---|---|---|
| Quartz (Q) | 27.65, 40.75, 62.75 | 3.22, 2.21, 1.48 |
| Feldspar (F) | 13.30, 15.1, 22.4, 31.1, 38.75, 42.25, 43.5, 46.05, 48.85, 50.25, 52.26, 55.00, 63.95, 65.45, 71.2 | 6.65, 5.86, 3.94, 2.87, 2.32, 2.14, 2.08, 1.97, 1.86, 1.81, 1.75, 1.67, 1.45, 1.42, 1.32, |
| Kaolinite (K) | 12.15, 19.7, 24.9, 34.05, 37.7, 41.1, 46.05, 54.25, 56.75, 63.95, 69.85 | 7.27, 4.5, 3.57, 2.63, 2.38, 2.19, 1.97, 1.69, 1.62, 1.45, 1.34 |
| Illite (I) | 21.35, 22.55, 29.85, 38.75, 41.1, 43.5, 46.05, 47.65, 54.25, 56.75, 58.15 | 4.16, 3.94, 2.99, 2.32, 2.19, 2.08, 1.97, 1.91, 1.69, 1.62, 1.58 |
| Augite (A) | 27.65, 34.95, 37.7, 40.75, 45.15, 46.05, 52.26, 55.0, 63.95, 73.55 | 3.22, 2.56, 2.38, 2.21, 2.01, 1.97, 1.75, 1.67, 1.45, 1.29 |
| Calcium aluminium silicate (CAS) | 13.3, 34.05, 35.95, 41.1, 44.9, 47.65, 58.15, 60.3 | 6.65, 2.63, 2.49, 2.19, 2.02, 1.91, 1.58, 1.53 |
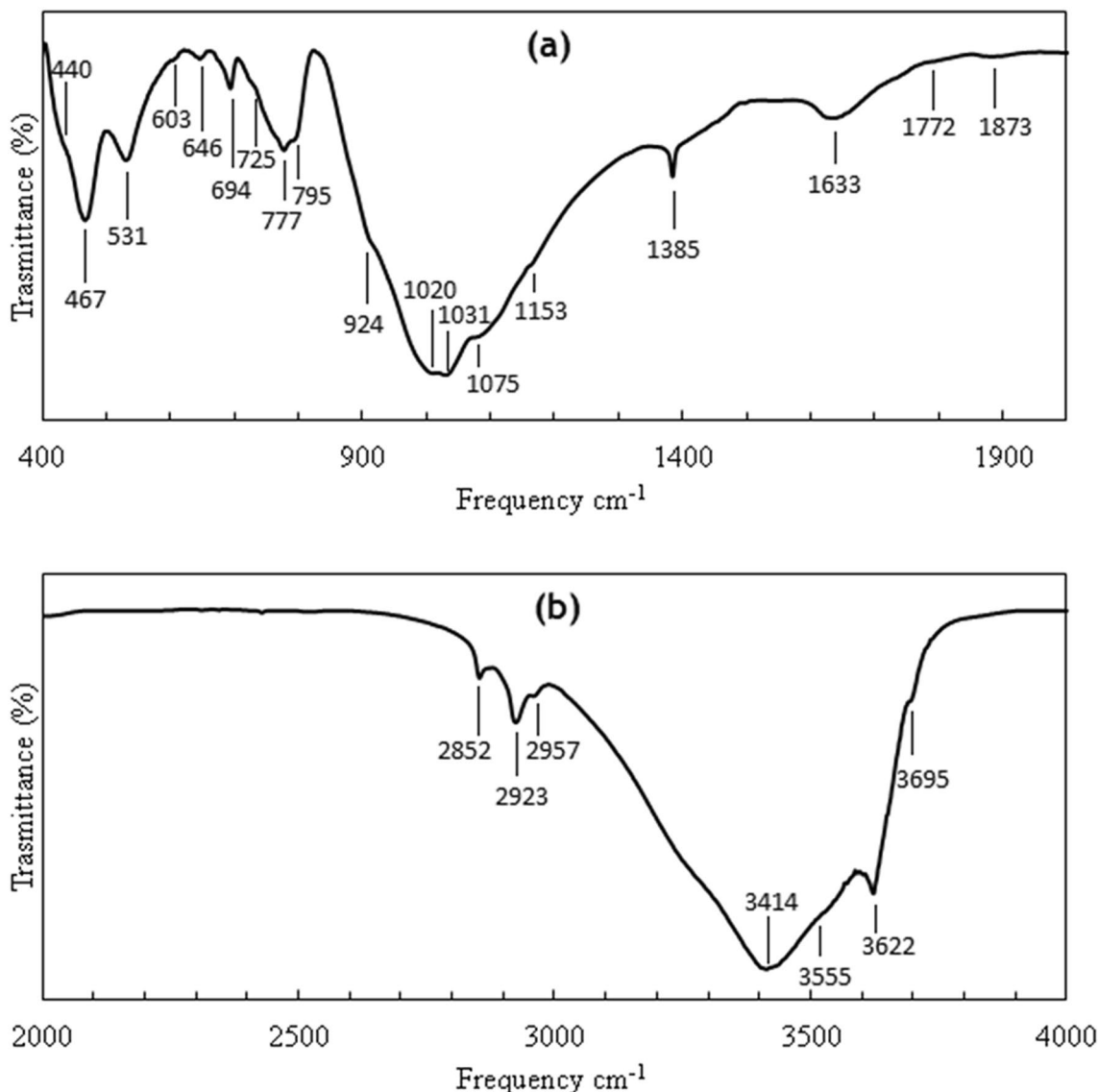
Fig. 9 FTIR spectrum of dust sample for the frequency range 400–4000 cm$^{-1}$. The spectrum is shown in two separate wave ranges, 400–1999 cm$^{-1}$ in (**a**) and 2000–4000 cm$^{-1}$ in (**b**)

**Table 4** The FTIR spectra peak observed with corresponding to the literature FTIR spectra peak for different minerals

| Minerals | Observed wave no. (cm$^{-1}$) | Related wave no. as per literature (cm$^{-1}$) | References |
|---|---|---|---|
| Feldspar | 440, 646, 725, 1772 | 440, 645, 648,727, 1772 | [51, 52] |
| Quartz | 467, 694, 778, 1075, 1153, 1873 | 465, 467, 468, 470, 693, 694, 695, 777, 780, 1077, 1087, 1144, 1164, 1872 | [20, 51–53] |
| Augite | 924, 1020 | 937, 1020 | [50] |
| Cerussite | 1385 | 1385 | [51] |
| Calcite | 1633, 2957 | 1636, 2982 | [51] |
| Organic carbon | 2852, 2923 | 2850, 2853, 2921, 2925 | [20, 51] |
| Clay minerals | | | |
| Kaolinite, illite, montmorillonite, imogolite | 531, 603, 795,1031, 3414, 3555, 3622, 3695 | 537, 602, 790, 795, 1032, 1033, 3405, 3550, 3620, 3623, 3629, 3694, 3695, 3698 | [20, 51, 53–55] |
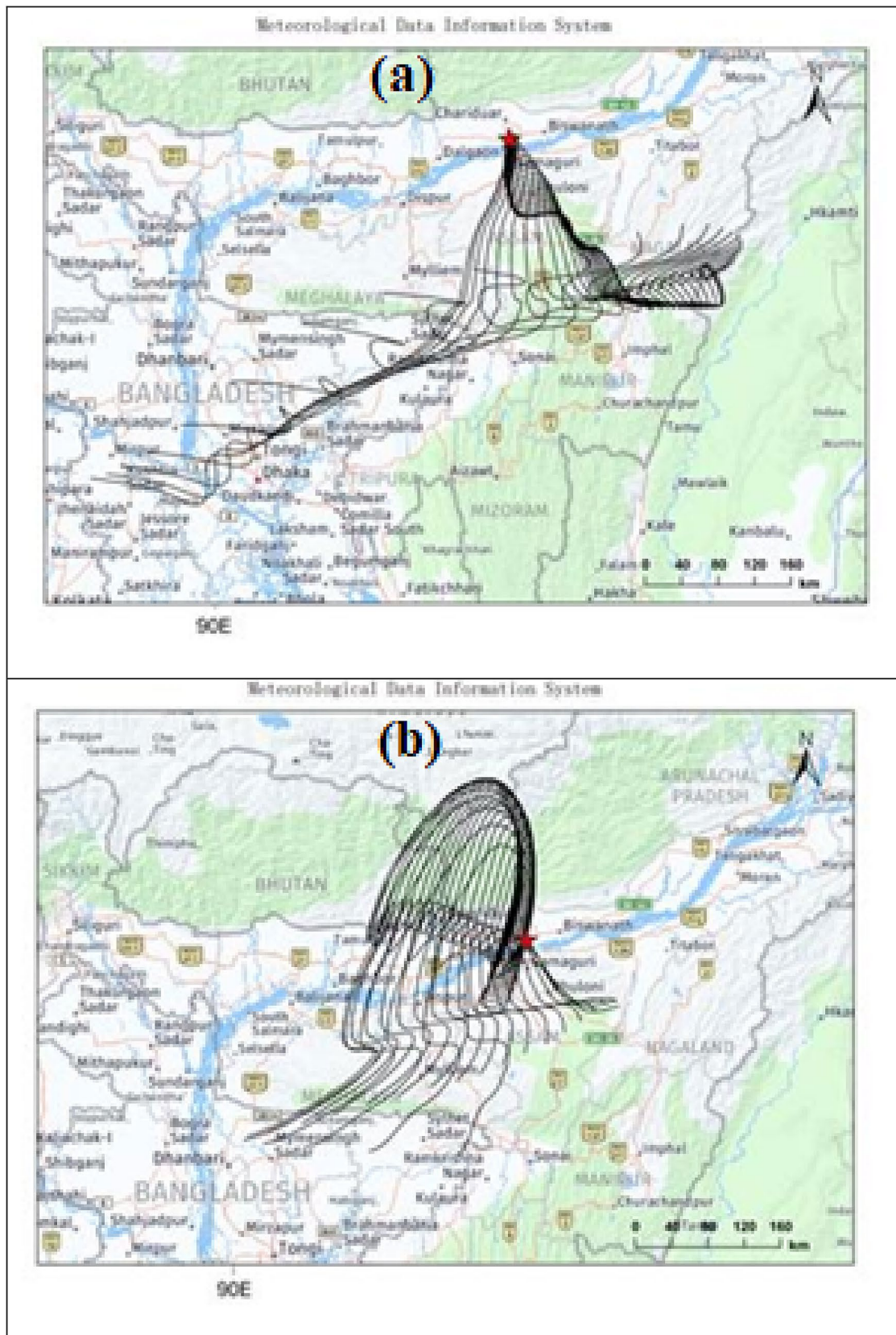
**Fig. 10** Airmass back trajectory clusters reaching Tezpur (the sampling station) of mid-Brahmaputra Valley

# 4 Conclusion

Morphology study showed that particles originated from geogenic and anthropogenic sources have mainly spherical and irregular shapes and particles from biogenic origin have a distinct spherical structure. Both fine and coarse particles were present in the atmospheric aerosol samples. Mineralogy study revealed dried beds of Brahmaputra River as a source of atmospheric aerosol particles during the windy events of pre-monsoon season. This is also supported by the presence of diatom in the samples. More detailed morphological study and chemical characterization in different seasons and different episodic periods over Brahmaputra Valley would reveal more information on atmospheric particles and associated sources.

## Compliance with ethical standards

**Conflict of interest** On behalf of all authors, the corresponding author states that there is no conflict of interest.

# References

1. Andreae MO (1996) Raising dust in the greenhouse. Nature 380(6573):389–390
2. Wurzler S, Reisin TG, Levin Z (2000) Modification of mineral dust particles by cloud processing and subsequent effects on drop size distributions. J Geophys Res Atmos 105(D4):4501–4512
3. Pope CA III, Dockery DW (2006) Health effects of fine particulate air pollution: lines that connect. J Air Waste Manag Assoc 56(6):709–742
4. USEPA. Criteria Air Pollutants. https://www.epa.gov/criteria-air-pollutants/naaqs-table. Accessed 4 June 2020
5. Gadi R, Sharma SK, Mandal TK (2019) Source apportionment and health risk assessment of organic constituents in fine ambient aerosols ($PM_{2.5}$): A complete year study over National Capital Region of India. Chemosphere 221:583–596
6. Yadav S, Gettu N, Swain B, Kumari K, Ojha N, Gunthe SS (2020) Bioaerosol impact on crop health over India due to emerging fungal diseases (EFDs): an important missing link. Environ Sci Pollut Res 27:12802–12829
7. Li W, Shao L, Zhang D, Ro CU, Hu M, Bi X, Geng H, Matsuki A, Niu H, Chen J (2016) A review of single aerosol particle studies in the atmosphere of East Asia: morphology, mixing state, source, and heterogeneous reactions. J Clean Prod 112:1330–1349
8. Coz E, Artíñano B, Robinson AL, Casuccio GS, Lersch TL, Pandis SN (2008) Individual particle morphology and acidity. Aerosol Sci Technol 42(3):224–232
9. Lee BK, Hieu NT (2013) Seasonal ion characteristics of fine and coarse particles from an urban residential area in a typical industrial city. Atmos Res 122:362–377
10. Agrawal A, Upadhyay VK, Sachdeva K (2011) Study of aerosol behavior on the basis of morphological characteristics during festival events in India. Atmos Environ 45(21):3640–3644
11. McDonald R, Biswas P (2004) A methodology to establish the morphology of ambient aerosols. J Air Waste Manag Assoc 54(9):1069–1078
12. Mishra SK, Saha N, Singh S, Sharma C, Prasad MV, Gautam S, Misra A, Gaur A, Bhattu D, Ghosh S, Dwivedi A (2017) Morphology, mineralogy and mixing of individual atmospheric particles over Kanpur (IGP): relevance of homogeneous equivalent sphere approximation in radiative models. MAPAN 32(3):229–241
13. Ebert M, Weinbruch S, Rausch A, Gorzawski G, Helas G, Hoffmann P, Wex H (2002) Complex refractive index of aerosols during LACE 98# x2010; as derived from the analysis of individual particles. J Geophys Res: Atmos 107(D21):LAC-3.
14. Jacobson MZ (2001) Strong radiative heating due to the mixing state of black carbon in atmospheric aerosols. Nature 409(6821):695–697
15. Berner A, Sidla S, Galambos Z, Kruisz C, Hitzenberger R, Ten Brink HM, Kos GP (1996) Modal character of atmospheric black carbon size distributions. J Geophys Res Atmos 101(D14):19559–19565
16. Ramanathan V, Crutzen PJ, Kiehl JT, Rosenfeld D (2001) Aerosols, climate, and the hydrological cycle. Science 294(5549):2119–2124
17. Winchester JW, Wang MX (1989) Acid-base balance in aerosol components of the Asia-Pacific region. Tellus B41(3):323–337
18. Soler R, Nicolás JF, Caballero S, Yubero E, Crespo J (2016) Depletion of tropospheric ozone associated with mineral dust outbreaks. Environ Sci Pollut Res 23(19):19376–19386
19. Weinzierl B, Ansmann A, Prospero JM, Althausen D, Benker N, Chouza F, Dollner M, Farrell D, Fomba WK, Freudenthaler V, Gasteiger J (2017) The Saharan aerosol long-range transport and aerosol–cloud-interaction experiment: overview and selected highlights. Bull Am Meteorol Soc 98(7):1427–1451
20. Neupane BB, Sharma A, Giri B, Joshi MK (2020) Characterization of airborne dust samples collected from core areas of Kathmandu Valley. Heliyon 6(4):e03791
21. Attiya AA, Jones BG (2020) Assessment of mineralogical and chemical properties of airborne dust in Iraq. SN App Sci 2(9):1–21
22. Engelbrecht JP, Moosmüller H, Pincock S, Jayanty RK, Lersch T, Casuccio G (2016) Mineralogical, chemical, morphological, and optical interrelationships of mineral dust re-suspensions. Atmos Chem Phy 16(17):10809
23. Buseck PR, Pósfai M (1999) Airborne minerals and related aerosol particles: effects on climate and the environment. PNAS 96(7):3372–3379

24. Mogo S, Cachorro VE, de Frutos AM (2005) Morphological, chemical and optical absorbing characterization of aerosols in the urban atmosphere of Valladolid. Atmos Chem Phys Eur Geosci Union 5(10):2739–2748

25. Hu W, Niu H, Zhang D, Wu Z, Chen C, Wu Y, Shang D, Hu M (2016) Insights into a dust event transported through Beijing in spring 2012: Morphology, chemical composition and impact on surface aerosols. Sci Total Environ 565:287–298

26. Lin CY, Lee YH, Kuo CY, Chen WC, Sheng YF, Su CJ (2018) Impact of river-dust events on air quality of western Taiwan during winter monsoon: Observed evidence and model simulation. Atmos Environ 192:160–172

27. Sharma AR, Kharol SK, Badarinath KVS (2009) Satellite observations of unusual dust event over North-East India and its relation with meteorological conditions. J Atmos Solar-Terr Phys 71(17–18):2032–2039

28. Pathak B, Kalita G, Bhuyan K, Bhuyan PK, Moorthy KK (2010) Aerosol temporal characteristics and its impact on shortwave radiative forcing at a location in the northeast of India. J Geophys Res: Atmos 115(D19):D19204

29. Deka P, Bhuyan P, Daimari R, Sarma KP, Hoque RR (2016) Metallic species in $PM_{10}$ and source apportionment using PCA-MLR modeling over mid-Brahmaputra Valley. Arab J Geosci 9(5):335

30. Bhuyan P, Barman N, Bora J, Daimari R, Deka P, Hoque RR (2016) Attributes of aerosol bound water soluble ions and carbon, and their relationships with AOD over the Brahmaputra Valley. Atmos Environ 142:194–209

31. Satsangi PG, Yadav S (2014) Characterization of $PM_{2.5}$ by X-ray diffraction and scanning electron microscopy–energy dispersive spectrometer: its relation with different pollution sources. Int J Environ Sci Technol 11(1):217–232.

32. Berry IG (1974) Selected powder diffraction data for mineralogy. JCPDS, Swanthmore, PA, USA

33. Prabhu V, Shridhar V, Choudhary A (2019) Investigation of the source, morphology, and trace elements associated with atmospheric $PM_{10}$ and human health risks due to inhalation of carcinogenic elements at Dehradun, an Indo-Himalayan city. SN Appl Sci 1(5):429

34. Rodríguez I, Galí S, Marcos C (2009) Atmospheric inorganic aerosol of a non-industrial city in the centre of an industrial region of the North of Spain, and its possible influence on the climate on a regional scale. Environ Geol 56(8):1551–1561

35. Wittmaack K (2005) Brochosomes produced by leafhoppers-a widely unknown, yet highly abundant species of bioaerosols in ambient air. Atmos Environ 39(6):1173–1180

36. Schroeder TB, Houghtaling J, Wilts BD, Mayer M (2018) It's not a bug, it's a feature: functional materials in insects. Adv Mater 30(19):1705322

37. Sofiev M, Siljamo P, Ranta H, Rantio-Lehtimäki A (2006) Towards numerical forecasting of long-range air transport of birch pollen: theoretical considerations and a feasibility study. Int J Biometeorol 50(6):392

38. Steiner AL, Brooks SD, Deng C, Thornton DC, Pendleton MW, Bryant V (2015) Pollen as atmospheric cloud condensation nuclei. Geophys Res Lett 42(9):3596–3602

39. Sonwani S, Kulshrestha U (2018) Morphology, elemental composition and source identification of airborne particles in Delhi. India J Indian Geophys Union 22(6):607–620

40. Deka P, Hoque RR (2014) Incremental effect of festive biomass burning on wintertime $PM_{10}$ in Brahmaputra Valley of Northeast India. Atmos Res 143:380–391

41. Bhuyan P, Deka P, Prakash A, Balachandran S, Hoque RR (2018) Chemical characterization and source apportionment of aerosol over mid Brahmaputra Valley, India. Environ Pollut 234:997–1010

42. Pipal AS, Jan R, Satsangi PG, Tiwari S, Taneja A (2014) Study of surface morphology, elemental composition and origin of atmospheric aerosols ($PM_{2.5}$ and $PM_{10}$) over Agra, India. Aerosol Air Qual Res 14(6):1685–1700.

43. Bhardwaj P, Singh BP, Pandey AK, Jain VK, Kumar K (2017) Characterization and morphological analysis of summer and wintertime $PM_{2.5}$ aerosols over urban-rural locations in Delhi-NCR. IJAES 12(5):1009–1030.

44. Falkovich AH, Ganor E, Levin Z, Formenti P, Rudich Y (2001) Chemical and mineralogical analysis of individual mineral dust particles. J Geophys Res Atmos 106(D16):18029–18036

45. Ismail KN, Hussin K, Idris MS (2007) Physical, chemical and mineralogical properties of fly ash. J Nucl Relat Technol 4:47–51

46. Zuo RF, Du GX, Yang WG, Liao LB, Li Z (2016) Mineralogical and chemical characteristics of a powder and purified quartz from Yunnan Province. Open Geosci 8(1):606–611

47. Van Der Plas L (2011) The identification of detrital feldspars. Elsevier, Amsterdam

48. Kodama H, Oinuma K (1962) Identification of kaolin minerals in the presence of chlorite by X-ray diffraction and infrared absorption spectra. Clays Clay Miner 11(1):236–249

49. Nowak S, Lafon S, Caquineau S, Journet E, Laurent B (2018) Quantitative study of the mineralogical composition of mineral dust aerosols by X-ray diffraction. Talanta 186:133–139

50. Hamadi A, Nabih K (2012) Alkali activation of oil shale ash based ceramics. J Chem 9(3):1373–1388

51. Kumar RS, Rajkumar P (2014) Characterization of minerals in air dust particles in the state of Tamilnadu, India through FTIR, XRD and SEM analyses. Infrared Phys Technol 67:30–41

52. Hlavay J, Jonas K, Elek S, Inczedy J (1978) Characterization of the particle size and the crystallinity of certain minerals by IR spectrophotometry and other instrumental methods—II. Investigations on quartz and feldspar. Clays Clay Miner 26(2):139–143.

53. Pickard KJ, Walker RF, West NG (1985) A comparison of X-ray diffraction and infra-red spectrophotometric methods for the analysis of α-quartz in airborne dusts. Ann Occup Hyg 29(2):149–167

54. Bishop JL, Pieters CM, Edwards JO (1994) Infrared spectroscopic analyses on the nature of water in montmorillonite. Clays Clay Miner 42(6):702–716

55. Ojima J (2003) Determining of crystalline silica in respirable dust samples by infrared spectrophotometry in the presence of interferences. J Occup Health 45(2):94–103

56. Kotoky P, Bezbaruah D, Baruah J, Borah GC, Sarma JN (2006) Characterization of clay minerals in the Brahmaputra river sediments, Assam, India. Curr Sci 91:1247–1250

57. Rahmanb MA, Biswasb PK, Zamanb MN, Miah MY, Hossain T, Huq SI (2012) Characterization of the sand of Brahmaputra river of Bangladesh. Bangladesh J Sci Ind Res 47(2):167–172

58. Biswas SP, Boruah S (2000) Fisheries ecology of the northeastern Himalayas with special reference to the Brahmaputra River. Ecol Eng 16(1):39–50

59. Saikia L, Mahanta C, Borah SB (2018) A novel approach to calculate braiding of a large alluvial river. Curr Sci 115(6):1179

60. Liu L, Shi P, Hu X, Liu T, Guo L, Zhang X, Tang Y, Lv Y, Sun B, Zhang G, Zhang X (2011) Natural factors influencing blown sand hazards in Beijing. Int J Disaster Risk Sci 2(2):23–31